Foreground Scaling in the BICEP/Keck 2018 Likelihood

University of Cincinnati
Physics & Astrophysics Capstone
Advisor: Colin Bischoff

Lauren Bell
August 2, 2023

Abstract

When studying B-mode polarization in the Cosmic Microwave Background, there is foreground emission from the Milky Way that obscures our view of the CMB. This foreground consists of dust and synchrotron radiation, where the foreground power spectra scales with angular scale. While this power-law is empirically supported when analyzing small patches of the sky, there is no theory to support this scaling. The baseline likelihood used in in the BK18 analysis uses data from multiple different telescopes, including the BICEP/Keck collaboration, WMAP, and Planck through the 2018 observation season. By using this data and separating dust and synchrotron radiation into bins based on angular scale, ℓ, and changing the likelihood calculation, we make the foreground model more flexible. The new likelihood follows the initial power-law likelihood within 1σ for both dust and synchrotron.

1 Background

1.1 CMB polarization and B-modes

The standard cosmological model, or the ΛCDM model, follows the expansion of the universe after the Big Bang. In the standard cosmological model, the universe went through a period of inflation that was near-exponential and has continued to expand under gravitational influence. The theory of inflation suggests that in the exponential expansion of the universe, the energy of the universe was divided into matter, radiation, and dark energy. The initially radiation dominated universe became matter dominated. After this began recombination, which is the emission of the Cosmic Microwave Background. The CMB shows the state of the universe less than a million years after the Big Bang and consists of remnant radiation that holds the fundamental features of the universe (Samtleben, Staggs, and Winstein 2007). The Cosmic Microwave Background provides the most theoretically strong cosmological constraints due to the sound theory behind it (Heavens 2008).

Polarization in the Cosmic Microwave Background can be separated into 2 modes. This separation is due to the distinct geometric patterns that each mode creates. Mathematically, Stokes parameters can be used to describe the polarization of electromagnetic radiation, separating Q polarization from U polarization. E-modes and B-modes are these two different components of the 2D polarization field seen when observing the CMB. When polarization is parallel or perpendicular to the gradient of the polarization, it is E-mode polarization, or Q polarization, but when it is crossed at a $\pm 45^\circ$ angle, it is B-mode, or U, polarization. Gravitational waves have both an E-mode and a B-mode polarization component. B-mode polarization is important because they can be targeted in the signal of inflation at very high sensitivity without significant E-mode detection. Detection of B-mode polarization at large angular scales provide confirmation of inflation because of inflationary gravitational waves that source B-modes around $\ell = 80$. "Models of inflation predict that gravitational waves will source B modes at angular scales of a degree or larger, but they don't predict the amplitude, which we parameterize with the tensor-to-scalar ratio, r" (Bischoff n.d.). The tensor to scalar ratio also is important in the detection of primordial B-mode polarization because it represents a direct connection to the scale of inflation (Abazajian et al. 2015).

1.2 Dust and Synchrotron Foregrounds

When trying to detect B-modes, there is diffuse matter in the way that emits microwaves that makes B-mode detection more difficult. The two classes of Galactic foreground are dust and synchrotron radiation. In synchrotron radiation, an electromagnetic radiation is emitted when an electron travels in a curved path in the Milky Way's magnetic field. The spectrum of synchrotron is a power law in frequency, which mostly reflects the energy distribution of electrons. Interstellar dust refers to microscopic, generally less than 1 μm pieces of matter, that will heat up in starlight and glow in microwaves. The dust spectrum in millimeter wavelength follows a modified blackbody law, where the usual blackbody spectrum is multiplied by a power law in frequency, ν^β. In this power law in frequency, $\beta \approx 1.5 - 1.6$. This accounts for the scaling of dust emissivity. These foregrounds are much brighter in the plane of the Milky Way, so we can target regions of the sky that are out of the plane. Since dust and synchrotron each have their own spectrum with frequency, which is different than the 2.73 K blackbody spectrum of the CMB, we can observe the sky at different frequencies and separate the CMB and foreground components.

1.3 Evidence for Power Law Scaling with ℓ

When studying B-modes, there is evidence that dust detection scales as a power law with ℓ. ℓ corresponds inversely with angular scale, $\theta = \frac{180^\circ}{\ell}$. This power scaling is shown clearly in Figure 1 from Planck Collaboration, Adam, et al. 2016, which analyzes 70%, 50%, and 30%

of the sky. The dust power spectrum in this figure is very well behaved at higher regions, but gets noisier in smaller regions and begin to depart from the power law behavior observed. This phenomenon is also shown in the Planck 2018 results, (Planck Collaboration, Akrami, et al. 2020), studying the cleanest 71% of the sky. As the area of the sky being analyzed reduces, the error bars increase significantly due to an increase in variance.

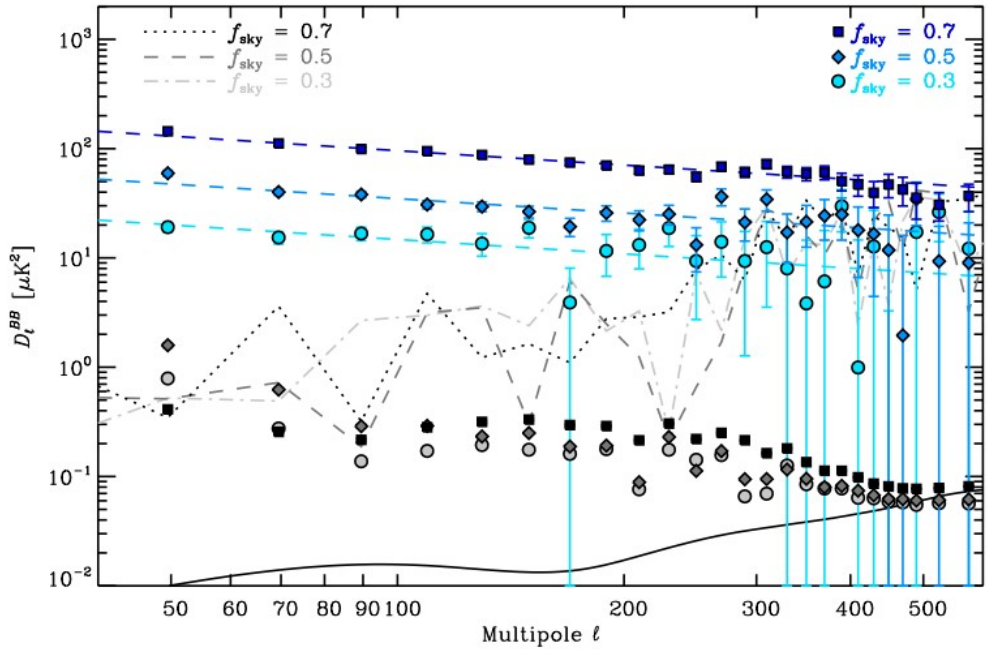

Figure 1: The D_ℓ^{BB} (blue, bottom) power spectra (in μK^2_{CMB}) is computed over three different analysis regions, $f_{sky} = 0.3$ (circles, lightest), $f_{sky} = 0.5$ (diamonds, medium), and $f_{sky} = 0.7$ (squares, darkest). Error bars are shown as $\pm\sigma$. The power law for each spectrum is represented as a dashed line of the corresponding color. The solid black line displays the $r = 0.2 D_\ell^{BB}$ CMB model, where the rise for ℓ is due to lensing contribution. The different shades of grey represent the global estimates of the power spectra of the systematic effects responsible for intensity-to-polarization leakage. The dotted and dashed lines each represent the null-test spectra anticipated, where a null test shows that any potential systematic effects in the data do not affect the computation of the spectrum amplitudes of D_ℓ^{BB} (Figure 2, Planck Intermediate Results, Planck Collaboration, Adam, et al. 2016)

The power law scaling in the full sky might obtain different results than an analysis of a small patch of sky. As shown in Figure 1, variance increases as the amount of sky being analyzed decreases. This significant increase in variance is shown between $f_{sky} = 0.7$ and $f_{sky} = 0.3$ in Figure 1. Given the increase in variance at smaller patches of the sky, when studying roughly 1.5% of the sky, which the BICEP-Keck XIII analysis does, we expect to have significantly increased variances. This gives reason to the idea that the scaling of foregrounds might not align with a power law at small observation areas.

2 BK18 Likelihood

2.1 Instrumentation in the BICEP/Keck Collaboration

BICEP2 is a telescope that is dedicated to looking for B-mode polarization from the CMB. The telescope has a 26 cm lens and 256 pairs of bolometers that are viewing CMB polarization at a single wavelength. This device was upgraded to BICEP3, which began operations

in 2016 and was designed to be complimentary to the Keck Array. The Keck Array consists of 5 telescopes similar to BICEP2, all mounted together and pointed at the same patch of the sky. The Keck Array operates at two different wavelengths and has a combined 1280 pairs of bolometers. The upgrades from BICEP2 to BICEP3 were significant, upgrading the telescope to a 68 cm lens with 1280 pairs of bolometers (Astrophysics n.d.). All of these telescopes operate from the Amundsen-Scott South Pole Station and focus their observations on 1.5% of the sky with low foregrounds. The observing frequencies of these are varied because it is critical for separating the CMB from the foregrounds. The BICEP2 telescope observed at 150 GHz, the Keck Array observes at 95, 150, and 220 GHz, and the BICEP3 telescope is observing at 95 GHz

2.2 Data Set and Power Spectra in Analysis

The data set contains data from 11 maps from multiple different telescopes, Keck Array, BICEP3, WMAP, and Planck, measuring at different frequencies ranging between 23 and 353 GHz. Finding the cross spectra of the maps requires taking the Fourier transform of map 1 multiplied by the complex conjugate of the Fourier transform of map 2, however, if map 1 = map 2, this is an auto spectrum. This will include both power spectra of the individual maps, as well as the cross spectra between pairs of maps.

This Fourier transformation acts as a spherical harmonic transform, from which we will receive an angular scale, direction, and wavelength. Polarized angular power spectra, generally denoted as C_ℓ^{EE} and C_ℓ^{BB}, ranges over the multipoles $20 < \ell < 350$.

2.3 Foreground Data Model

For this project, we want a model that is based on cosmological and foreground parameters and will predict expectation values for all of the auto and cross spectra. The model created in the "The Latest Constraints on Inflationary B-modes from the BICEP/Keck Telescopes" has a model that fits these specifications (BICEP/Keck Collaboration et al. 2022). In the BK18 foreground model, dust amplitude is evaluated at 353 GHz and $\ell = 80$. Dust frequency spectral behavior is shown as a modified black body spectrum with a temperature of $T_{dust} = 19.6K$ and a frequency spectral index of β_{dust}. For dust, the spatial power spectrum is a power law where the power law scales with α_{dust} and $D_\ell \propto \ell^{\alpha_{dust}}$. In this model, $D_\ell \equiv \ell(\ell+1)C_\ell/2\pi$. For the synchrotron foreground model, amplitude is evaluated at 23 GHz and $\ell = 80$. This model assumes a simple power law for the spectral behavior, with $A_{sync} \propto \nu^{\beta_{sync}}$. The spatial power spectrum is shown as another power law, $D_\ell \propto \ell^{\alpha_{sync}}$. In both the synchrotron and dust foreground models, the power law scaling variable, α, ranges between $-1 < \alpha < 0$ (Ade et al. 2021). Combining these foreground models, the BK18 likelihood models the scaling of foreground dust and synchrotrons as:

$$D_{\ell,BB}^{\nu_1\nu_2} = A_d f_d^{\nu_1} f_d^{\nu_2} (\frac{\ell}{80})^{\alpha_d} + A_s f_s^{\nu_1} f_s^{\nu_2} (\frac{\ell}{80})^{\alpha_s} + \epsilon\sqrt{A_d A_s}(f_d^{\nu_1} f_s^{\nu_2} + f_d^{\nu_2} f_s^{\nu_1})(\frac{\ell}{80})^{\frac{\alpha_d+\alpha_s}{2}} \quad (1)$$

In this equation, A represents the amplitude, f is the frequency scaling for spectral energy density, $\nu_1 = 353GHz$, $\nu_2 = 23GHz$, α is the power law scaling index, and ϵ is the dust-synchrotron correlation factor, where all of the variables have the respective subscripts for dust or synchrotrons (BICEP/Keck Collaboration et al. 2022). Equation 1 is a cross spectrum between the dust and synchrotron spectra. The first component of the equation is the dust spectrum, the second component represents the synchrotron spectrum, and the final component is the dust-sync correlation spectrum. While Equation 1 has the requirements that we want for a foreground angular power model, we will be changing it for this project. By replacing the power law dependence with step-wise functions in ℓ in the likelihood, we are able to make the foreground analysis more flexible.

2.4 Calculating the Likelihood Using Bayesian Statistics

The BICEP/Keck 2018 analysis of this data set uses the Hamimeche-Lewis approximation (Hamimeche and Lewis 2008) that is applied to the cross-spectra taken from the maps used in the data set. By comparing observed bandpower for values $20 < \ell < 330$, there will be 9 bandpowers per spectrum and an eight parameter foreground model is created (Ade et al. 2021).

To explore the likelihood, a program using CosmoMC, now called Cobaya (Torrado and Lewis 2021), runs with an input of an initial guess for each parameter and samples the probability distribution to explore the priors in the BK18 likelihood. The program refines the initial guess to a covariance matrix using a Markov chain Monte Carlo sampler function (Lewis and Bridle 2002). MCMC simulations use Bayesian statistics to provide parameter estimations and explore the posterior distribution. A single set of parameters is required for the MCMC to calculate the probability. Given an initial point, the sampler assesses the convergence between different chains and provides a covariance matrix of the proposal posteriors. The MCMC sampler works by taking steps and evaluating the probability that the step from the initial guess is more or less probable. The sampler will finish running once it converges to a chosen accuracy, $R - 1$.

3 Results

3.1 Motivation

The current foreground model from the 2018 BICEP/Keck Collaboration is fit to a modified black body spectrum for the dust component and a power law in frequency for the synchrotron component, this has good motivation behind it. However, there is empirical support for the foreground angular power spectra scaling with ℓ in full sky observation averages, but there is no theoretical reasoning behind it for observing in small regions. Making the assumption that the dust and synchrotron angular power foregrounds do not scale on a smooth power law with respect to ℓ and aligns more with varying scaling at different sections, or bins, of ℓ. In Equation 1, the α variable represents the power index that the spectrum follows. To change the BK18 foreground likelihood, we change this equation to get rid of the α variable completely, thus taking away the entire power law function, and add ℓ bins instead. Changing the likelihood in this way will make the foreground analysis more flexible, then allowing the bin number and sizes to change if needed.

Initially, we chose six ℓ bins for both dust and synchrotrons. These ℓ bins ranged from 20-65, 65-120, 120-180, 180-250, 250-320, 320-600. After significant and clear dust amplitude detection in many bins, the dust scaling with ℓ bins remains the same. Synchrotrons were not detected significantly across 6 ℓ bins, so the number of bins was lowered from n=6 to n=2. After lowering these ℓ bins from the initial six, the new bins range from 20-120 and 120-600, representing low ℓ and high ℓ. Dust-synchrotron correlation factor, ϵ, which has a constant value across all ℓ and remains the same in the current analysis. The scaling with frequency, f_d^ν and f_s^ν, will also remain the same in the updated model. After changing this likelihood to include ℓ bins, we run the Markov Chain Monte Carlo sampler to find the amplitudes of dust and synchrotrons, along with the correlation between each parameter. In this project, the function is run at 95% accuracy, where $R - 1 = 0.05$.

3.2 Dust and Synchrotron Posterior Probability Distributions

The triangle plot shows the joint and marginalized posterior probability distributions of the parameters that are put into the MCMC sampler. This plot consists of 1D marginalized posterior distributions and joint 2D posterior distributions. In the 2D posterior distributions, the darker contour represents the 1σ, or 68%, of the distribution and the lighter contour represents the 2σ, or 95%, of the distribution.

The initial results of the data we analyzed are depicted in a triangle plot using the detDist function in Cobaya. Including all parameters, this results in a 12x12 dimension triangle plot that shows correlation between each parameter. Separating these results into two different triangle plots, we get Figure 2 and Figure 3,

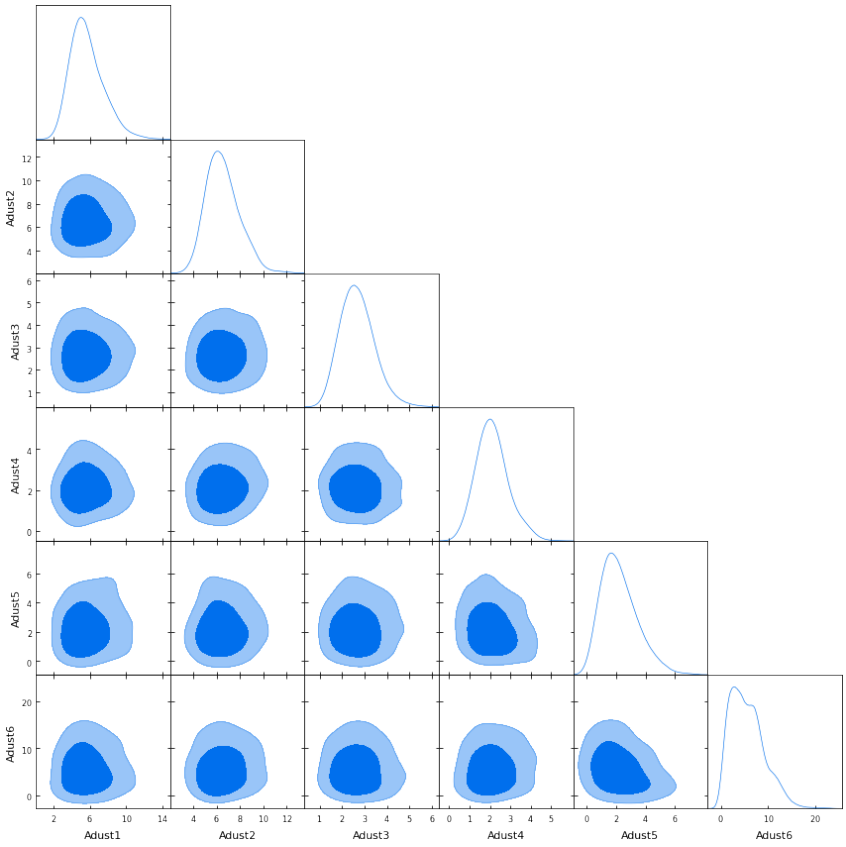

Figure 2: Triangle plot with only dust correlations and amplitudes, separated by ℓ bins

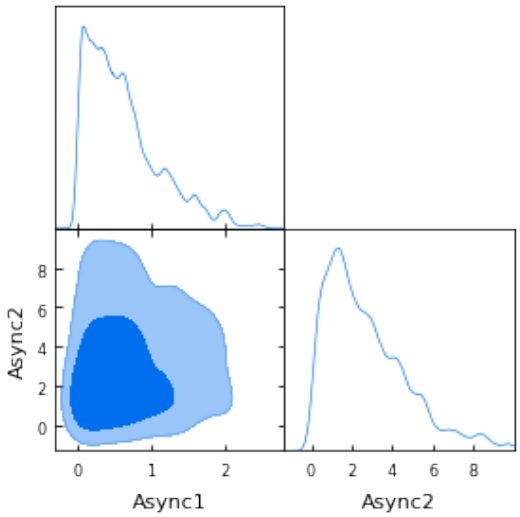

Figure 3: Triangle plot with only synchrotron correlations and amplitudes, separated by ℓ bins

Shown in Figure 2, detection of dust amplitude is significant but there is no significant correlation between dust in each ℓ bins, while in Figure 3 there is no consistent or significant synchrotron amplitude detection or correlation. While there is no correlation between synchrotron bins or dust bins, what about correlation between dust and synchrotrons? After we found amplitudes and correlations of dust and synchrotrons separately, we were able to find the 1D marginalized posterior plot for the dust-synchrotron correlation parameter.

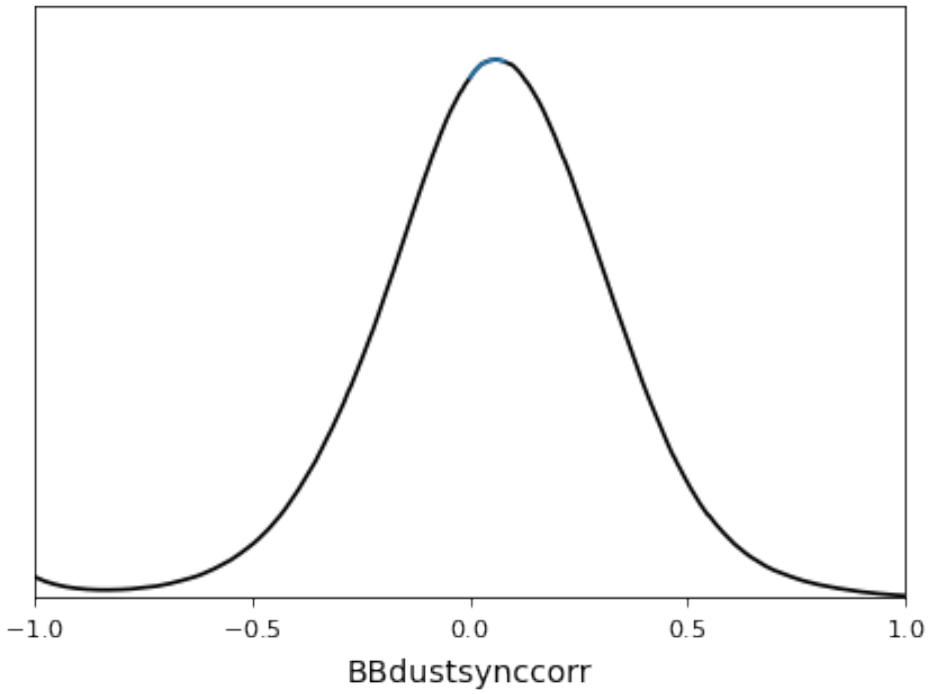

Figure 4: 1D marginalized posterior plot for the correlation between dust and synchrotrons.

In Figure 4, the correlation between dust and synchrotrons is shown as a posterior probability plot. The mean of the dust synchrotron plot is 0.0529, so there is not significant proof that synchrotron and dust spectra correlate in the foreground model.

3.3 A_{dust} vs ℓ and A_{sync} vs ℓ

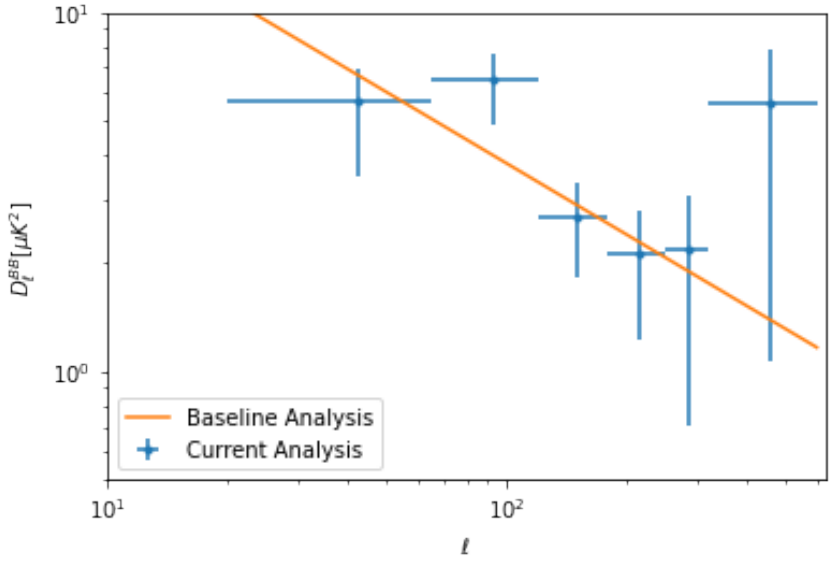

Figure 5: Compares the current dust foreground model against the power-law that the BK18 analysis expected as a baseline scale on a log-log plot. Vertical error bars depict the 1σ area, while the horizontal bars show the range of each dust bin per point. The power spectrum from the baseline analysis follows the curve $D_\ell^{BB} = 4.4 * \frac{\ell}{80}^{-0.66}$

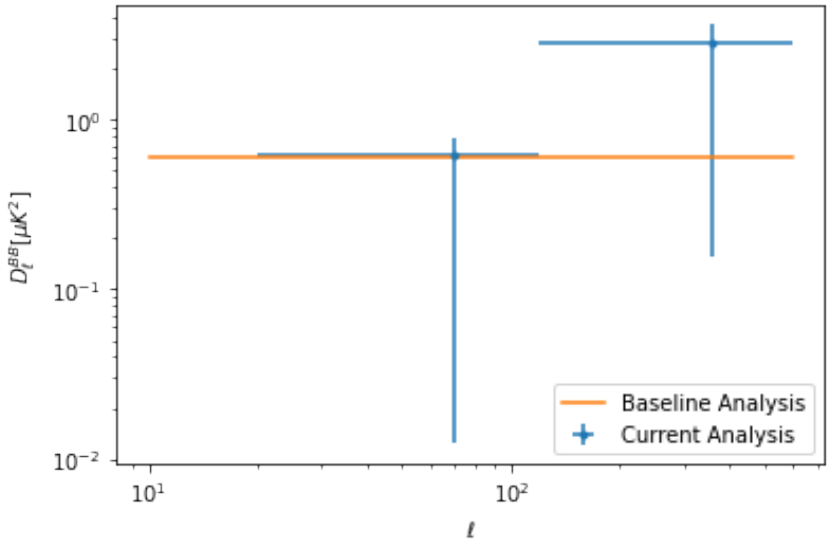

Figure 6: Compares the current synchrotron foreground model against the power-law that the BK18 analysis expected as a baseline scale on a log-log plot. Vertical error bars depict the 1σ area, while the horizontal bars show the range of each synchrotron bin per point. The power spectrum from the baseline analysis follows the curve $D_\ell^{BB} = 0.6 * \frac{\ell}{80}^{0}$

Figures 5 and 6 compare the power-law used in the BK18 baseline likelihood to the binned method we used in this project. The vertical error bars in Figures 5 and 6 come from the

1σ area of the 1D marginalized plots, Figures 2 and 3. In both figures, the power-law lines up well with the binned method that we used. In Figure 5, each ℓ bin is within 1σ except the $65 < \ell < 120$. This gives reasonable confirmation that the new likelihood ??

3.4 Marginalized Posterior for r in the BK18 Baseline and Current Analysis

In the BK18 likelihoods, both for the current project and the initial likelihood that we started with, the variable r represents the tensor-to-scalar ratio. CMB primordial tensor B-mode power scales linearly with r and the BK18 likelihood uses data to constrain this r parameter.

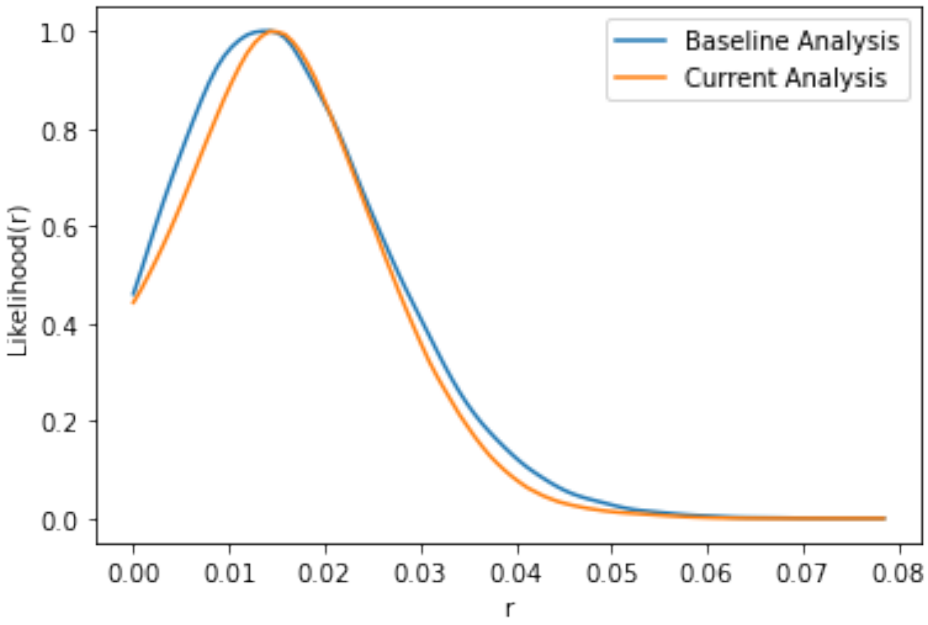

Figure 7: r Likelihood in Capstone vs. BK18 Data Baseline Analysis. The BK18 analysis peaks at r = 0.011, while the current analysis peaks at r = 0.015. The mean of r in the baseline analysis is 0.0393, while the mean in the current analysis is 0.01689.

4 Conclusion

Analyzing the BK18 data with the MCMC sampler, we see significant and consistent dust detection but there is no significant synchrotron detection. This allows for a more efficient likelihood to be made, with less bins to analyze synchrotrons. After creating a new likelihood and changing it to fit the foreground model, then analyzing it, we see that this likelihood results in a similar accuracy as the power-law, roughly within 1σ in Figures 5 and 6. Making the foreground likelihood more flexible provides theory behind the foreground likelihood when analyzing small patches of the sky, where this project studies 1.5% of the sky. The likelihood that we changed resulted in similar constraint to the r parameter, so the updated likelihood provides similar accuracy to the baseline likelihood when studying the amplitude of B-mode signal.

References

[1] K. N. Abazajian et al. "Inflation physics from the cosmic microwave background and large scale structure". In: *Astroparticle Physics* 63 (Mar. 2015), pp. 55–65. DOI: 10.1016/j.astropartphys.2014.05.013. arXiv: 1309.5381 [astro-ph.CO].

[2] P. A. R. Ade et al. "Improved Constraints on Primordial Gravitational Waves using Planck, WMAP, and BICEP/Keck Observations through the 2018 Observing Season". In: 127.15, 151301 (Oct. 2021), p. 151301. DOI: 10.1103/PhysRevLett.127.151301. arXiv: 2110.00483 [astro-ph.CO].

[3] Harvard Smithsonian Center for Astrophysics. *BICEP*. URL: https://pweb.cfa.harvard.edu/facilities-technology/telescopes-instruments/bicep.

[4] BICEP/Keck Collaboration et al. "The Latest Constraints on Inflationary B-modes from the BICEP/Keck Telescopes". In: *arXiv e-prints*, arXiv:2203.16556 (Mar. 2022), arXiv:2203.16556. DOI: 10.48550/arXiv.2203.16556. arXiv: 2203.16556 [astro-ph.CO].

[5] Colin Bischoff. *CMB Polarization*. URL: https://lweb.cfa.harvard.edu/~cbischoff/cmb/#:~:text=Gravitational%20waves%20from%20inflation%20can,by%20the%20larger%20E-modes..

[6] Samira Hamimeche and Antony Lewis. "Likelihood analysis of CMB temperature and polarization power spectra". In: 77.10, 103013 (May 2008), p. 103013. DOI: 10.1103/PhysRevD.77.103013. arXiv: 0801.0554 [astro-ph].

[7] A Heavens. "The cosmological model: an overview and an outlook". In: *Journal of Physics: Conference Series* 120.2 (July 2008), p. 022001. DOI: 10.1088/1742-6596/120/2/022001. URL: https://dx.doi.org/10.1088/1742-6596/120/2/022001.

[8] Antony Lewis and Sarah Bridle. "Cosmological parameters from CMB and other data: A Monte Carlo approach". In: 66.10, 103511 (Nov. 2002), p. 103511. DOI: 10.1103/PhysRevD.66.103511. arXiv: astro-ph/0205436 [astro-ph].

[9] Planck Collaboration, R. Adam, et al. "Planck intermediate results. XXX. The angular power spectrum of polarized dust emission at intermediate and high Galactic latitudes". In: 586, A133 (Feb. 2016), A133. DOI: 10.1051/0004-6361/201425034. arXiv: 1409.5738 [astro-ph.CO].

[10] Planck Collaboration, Y. Akrami, et al. "Planck 2018 results. XI. Polarized dust foregrounds". In: 641, A11 (Sept. 2020), A11. DOI: 10.1051/0004-6361/201832618. arXiv: 1801.04945 [astro-ph.GA].

[11] Dorothea Samtleben, Suzanne Staggs, and Bruce Winstein. "The Cosmic microwave background for pedestrians: A Review for particle and nuclear physicists". In: *Ann. Rev. Nucl. Part. Sci.* 57 (2007), pp. 245–283. DOI: 10.1146/annurev.nucl.54.070103.181232. arXiv: 0803.0834 [astro-ph].

[12] Jesú s Torrado and Antony Lewis. "Cobaya: code for Bayesian analysis of hierarchical physical models". In: *Journal of Cosmology and Astroparticle Physics* 2021.05 (May 2021), p. 057. DOI: 10.1088/1475-7516/2021/05/057. URL: https://doi.org/10.1088%2F1475-7516%2F2021%2F05%2F057.